INTEGRAL FIELD SPECTROSCOPY OF SUPERNOVA EXPLOSION SITES: CONSTRAINING THE MASS AND METALLICITY OF THE PROGENITORS. I. TYPE Ib AND Ic SUPERNOVAE

Hanindyo Kuncarayakti[1,2,3], Mamoru Doi[2,4], Greg Aldering[5], Nobuo Arimoto[6,7],
Keiichi Maeda[1], Tomoki Morokuma[2], Rui Pereira[8], Tomonori Usuda[7], and Yasuhito Hashiba[2,3]

[1] Kavli Institute for the Physics and Mathematics of the Universe (WPI), Todai Institutes for Advanced Study, The University of Tokyo,
5-1-5 Kashiwanoha, Kashiwa, Chiba 277-8583, Japan; hanindyo.kuncarayakti@ipmu.jp
[2] Institute of Astronomy, Graduate School of Science, The University of Tokyo, 2-21-1 Osawa, Mitaka, Tokyo 181-0015, Japan
[3] Department of Astronomy, Graduate School of Science, The University of Tokyo, 7-3-1 Hongo, Bunkyo-ku, Tokyo 113-0033, Japan
[4] Research Center for the Early Universe, The University of Tokyo, 7-3-1 Hongo, Bunkyo-ku, Tokyo 113-0033, Japan
[5] Physics Division, Lawrence Berkeley National Laboratory, 1 Cyclotron Road, Berkeley, CA 94720, USA
[6] National Astronomical Observatory of Japan, 2-21-1 Osawa, Mitaka, Tokyo 181-0015, Japan
[7] Subaru Telescope, National Astronomical Observatory of Japan, 650 North A'ohoku Place, Hilo, HI 96720, USA
[8] CNRS/IN2P3, Institut de Physique Nucléaire de Lyon, 4 Rue Enrico Fermi, F-69622 Villeurbanne Cedex, France
Received 2012 October 4; accepted 2013 May 1; published 2013 July 12

ABSTRACT

Integral field spectroscopy of 11 Type Ib/Ic supernova (SN Ib/Ic) explosion sites in nearby galaxies has been obtained using UH88/SNIFS and Gemini-N/GMOS. The use of integral field spectroscopy enables us to obtain both spatial and spectral information about the explosion site, enabling the identification of the parent stellar population of the SN progenitor star. The spectrum of the parent population provides metallicity determination via strong-line method and age estimation obtained via comparison with simple stellar population models. We adopt this information as the metallicity and age of the SN progenitor, under the assumption that it was coeval with the parent stellar population. The age of the star corresponds to its lifetime, which in turn gives the estimate of its initial mass. With this method we were able to determine both the metallicity and initial (zero-age main sequence) mass of the progenitor stars of SNe Ib and Ic. We found that on average SN Ic explosion sites are more metal-rich and younger than SN Ib sites. The initial mass of the progenitors derived from parent stellar population age suggests that SN Ic has more massive progenitors than SN Ib. In addition, we also found indication that some of our SN progenitors are less massive than $\sim$25 $M_\odot$, indicating that they may have been stars in a close binary system that have lost their outer envelope via binary interactions to produce SNe Ib/Ic, instead of single Wolf–Rayet stars. These findings support the current suggestions that both binary and single progenitor channels are in effect in producing SNe Ib/Ic. This work also demonstrates the power of integral field spectroscopy in investigating SN environments and active star-forming regions.

Key words: stars: massive – supernovae: general

Online-only material: color figures

1. INTRODUCTION

A great number of supernovae (SNe) have been observed and new ones are being discovered owing to ongoing transient surveys and monitorings. Despite the large, growing number of observed events the real nature of the progenitor of each type of SN is still not very well understood.

Recently, a number of core-collapse supernovae (CCSNe) have had their progenitor star detected in high-resolution pre-explosion images (e.g., Van Dyk et al. 2012; Fraser et al. 2011; Elias-Rosa et al. 2011; see Smartt 2009 for a review). The detection of the progenitor in several passbands enables a comparison between the observed colors and luminosity of the star with stellar models. While direct detection is obviously desirable, in most cases only upper luminosity limits could be derived due to non-detection. This, however, is still useful for constraining the progenitor properties. Comparison with theoretical models yields the evolutionary stage and position in the Hertzsprung–Russell diagram of the star from which the initial mass can ultimately be derived. Using this method, Smartt et al. (2009) conclude that SNe II-P arise from red supergiant stars with an initial mass between $8.5^{+1}_{-1.5}$ and $16.5 \pm 1.5\ M_\odot$.

While the progenitors of SNe II-P have been convincingly detected and characterized, currently no Ib/Ic progenitor has been detected. It is widely believed that since SNe Ib/Ic are deficient in hydrogen and helium, the most likely candidate for their progenitors would naturally be the Wolf–Rayet (WR) stars (Crowther 2007). Numerous stellar evolution models have been proposed to characterize the progenitor stars of different SN types (e.g., Heger et al. 2003; Eldridge & Tout 2004; Georgy et al. 2009) but these predictions are still not very well tested with observational data. Progenitor discoveries could provide useful comparisons but the number of data points is still too small and not very reliable, considering a number of uncertainties such as metallicity assumption and also the sensitivity of the method to errors in luminosity (determined using host galaxy distance) and the end state of the evolution of the exploding star. Furthermore, progenitor discoveries ideally should be followed up by post-explosion observation to ensure that the purported progenitor has indeed gone. However, this has not been done for the majority of the progenitors; thus, future confirmation of their disappearance is still needed.

The initial mass of a progenitor star is generally considered to be the most influential parameter driving the evolution of the star. Hydrogen-deficient (Type Ib, Ic) SNe require progenitors with high mass-loss rates to remove the outer hydrogen envelope of the star, in which metallicity-driven wind (e.g., Vink et al. 2001) or other mechanism could play a significant role. Therefore, it is also important to investigate the metallicity of the progenitor star in addition to the initial mass. This dependence on metallicity

affects the number ratio $N_{Ib/Ic}/N_{II}$ as suggested by several previous studies (Prantzos & Boissier 2003; Boissier & Prantzos 2009; Eldridge et al. 2008). Another possible mechanism of mass loss is via close binary interaction (e.g., Podsiadlowski et al. 1992). Extending the work of Smartt et al. (2009) for SN Ib/Ic progenitors, Eldridge et al. (2013) suggest that the non-detection of SN Ib/Ic progenitors may be explained by the idea that most of the SN Ib/Ic progenitors probably arise from interacting binaries with masses $\lesssim 20\,M_\odot$. An example where a binary scenario provides a good alternative explanation to the massive single star progenitor is given by Crockett et al. (2007) in the case of SN Ic 2002ap. From the analysis of pre-explosion images, they suggest that the progenitor of SN 2002ap was probably initially a 30–40 $M_\odot$ star with twice the standard mass-loss rate, or in a binary system as a 15–20 $M_\odot$ star.

Anderson et al. (2010) showed that SNe Ib/Ic occur in higher-metallicity environments than SNe II. High-metallicity massive stars tend to explode as SNe Ib/Ic, thus a higher number ratio $N_{Ib/Ic}/N_{II}$ is expected in higher-metallicity environment. While Anderson et al. (2010) suggest that SNe Ib and Ic have similar metallicities, Modjaz et al. (2011) argue that SNe Ic have higher metallicities than Ib. The results of Leloudas et al. (2011), and recently Sanders et al. (2012), also show indications of higher metallicities for Ic, but those results were not statistically significant. In contrast with this work, the previous studies mentioned above used slit spectroscopy to obtain spectra of the SN explosion sites from which the site metallicities were derived.

Considering the limitations of finding SN progenitors in high-quality pre-explosion images, several alternative methods have been devised to obtain insight into the nature and possible mass range of the progenitors. A statistical study by Anderson & James (2008) using correlations of SN positions within host galaxies with Hα emission showed that the association of SNe with recent star formation follows a SN Ic > Ib > II sequence, indicating a grouping of decreasing progenitor mass. This result is further reinforced in Anderson et al. (2012), but see Crowther (2013) for a discussion on how SN association with a nearby H II only weakly constrains the progenitor mass. Leloudas et al. (2011) suggest that SN Ib/Ic progenitors are more massive than 25–30 $M_\odot$ from the age of the youngest stellar population at the explosion site, estimated using the Hα emission line equivalent width (EW). However, in that case it is likely that multiple stellar populations have been observed and treated as a single one since the study used integrated light over a large region within the spectrograph slit, in some cases $\sim$1 kpc. Some of their targets are also not the exact explosion sites but other regions several kiloparsecs away in the host galaxy. Therefore, consequently, the real parent population might have been contaminated by other populations of possibly different ages and metallicities. This problem is also present in similar studies such as Modjaz et al. (2011) and Sanders et al. (2012). Here we endeavor to refine the results of those efforts by resolved spectroscopy of the explosion site with a typical spatial resolution of around 70 pc (1″ at 15 Mpc). A similar approach has been employed by Gogarten et al. (2009) to estimate the initial mass of the progenitor of the optical transient NGC 300 OT2008-1. They probed a region $\sim$50 pc around the transient, and determined an initial progenitor mass of 12–25 $M_\odot$ from an analysis of the stellar population at the site.

In this paper we report the results of our study of 11 nearby SN Ib/Ic explosion sites in which the parent stellar populations were detected and used to derive the progenitor star's mass and metallicity. We will use the terms star cluster, H II region, and OB association interchangeably in this paper to refer to the stellar population. As stars are born in clusters (Lada & Lada 2003; also see Bressert et al. 2010 who suggest that this depends on the adopted cluster definition, which may change the fraction of stars born in clusters to $\sim$45%–90%) and there is evidence that all massive stars may be born within clustered environments (Portegies Zwart et al. 2010), it is reasonable to derive a coeval star's age and metallicity from its parent stellar population. It is not expected that the progenitor star would have wandered far from the birthplace cluster since it would not have much time to travel before exploding as an SN—thus the parent cluster may be studied to extract useful information about the coeval SN progenitor star. The typical velocity dispersion inside a star cluster is a few km s^{-1} (Bastian & Goodwin 2006; Portegies Zwart et al. 2010), which corresponds to about a few pc Myr^{-1}. Therefore, an SN progenitor that belongs to such a cluster, if unbound, would only typically travel a few tens of parsecs during its several-megayear lifetime. By studying the host cluster, we were able to derive the initial masses and metallicities of the SN progenitors.

This paper is organized as follows. Observations, data reductions, and the subsequent analysis are presented in Section 2. Descriptions of the SN explosion sites are given in Section 3. We discuss our findings in Section 4, and, finally, a summary is presented in Section 5.

2. DATA ACQUISITION AND ANALYSIS METHOD

We selected our samples from the Asiago Supernova Database (Barbon et al. 1999). SNe in host galaxies with a radial velocity of 3000 km s^{-1} or less were selected and subsequent careful visual inspections of Digitized Sky Survey and Sloan Digital Sky Survey images of the explosion sites were performed using ALADIN.[9] We use equatorial coordinates from the Asiago database to locate the SN positions in the images. In addition, we also used the published images of the SN environment/light echo study by Boffi et al. (1999) to compare with and identify some SN host clusters. SN classification follows the Asiago database classification; in this paper, we present the study of our SN Ib/Ic samples while SNe II are presented in Kuncarayakti et al. (2013, hereafter Paper II).

SNe showing close association with a bright knot were selected as observation targets. We interpret these knots as the parent stellar population of the SN progenitor star. The utilization of broadband images ensures that there is no selection preference toward very young stellar populations, as opposed to if we carried out our selection using Hα or UV images. Therefore, we expect very little age bias to be present in our sample explosion site.

We observed seven of our targets in 2010–2011 using the SuperNova Integral Field Spectrograph (SNIFS; Aldering et al. 2002; Lantz et al. 2004) mounted at the University of Hawaii 2.2 m telescope (UH88) at Mauna Kea. Table 1 contains the observations of our SN site targets. The positional uncertainty of each SN is also shown; the reasons for each estimate are given in the description of each explosion site.

The integral field spectrograph SNIFS employs a fully filled 15×15 lenslet array in the integral field unit (IFU), covering a $6\overset{''}{.}4 \times 6\overset{''}{.}4$ field of view (FoV). The corresponding spatial resolution is 0.43 arcsec per spatial pixel (spaxel). SNIFS has a

---

Table 1
Target SN Site IFU Observations

SN	Type	R.A. (2000)	Decl. (2000)	$\sigma_{\alpha,\delta}$	Galaxy (N_{SN})	d [a] (Mpc)	Obs. Date[b]	Inst.[c]	Exposure	Seeing
1964L	Ic	11:52:49.09	+44:07:45.4	±2″	NGC 3938 (3)	17.4	2011 Mar 13	S	1800 s × 2	0″.8
1994I	Ic	13:29:54.07	+47:11:30.5	±1″	NGC 5194 (4)	7.9	2011 Mar 10	S	1800 s × 2	1″.1
2000ew	Ic	11:40:58.52	+11:27:55.9	±0″.7	NGC 3810 (2)	17.8	2011 Mar 15	S	1800 s × 2	0″.9
2004gt	Ic	12:01:50.37	−18:52:12.7	±0″.005	NGC 4038 (4)	20.9	2011 Mar 10	S	1800 s × 2	1″.2
2007gr	Ic	02:43:27.98	+37:20:44.7	±0″.02	NGC 1058 (3)	7.7	2011 Sep 29	G	1800 s × 4	0″.5
2009em	Ic	00:34:44.53	−08:23:57.6	±1″	NGC 157 (1)	19.5	2011 Sep 29	G	1800 s × 2	0″.6
1983N	Ib	13:36:51.23	−29:54:01.7	±0″.6	NGC 5236 (5)	6.9	2011 Mar 11	S	1800 s × 1	1″.5
1984L	Ib	02:35:30.54	−07:09:30.3	±0″.3	NGC 991 (1)	18.8	2011 Sep 29	G	2700 s × 2	0″.6
1999ec	Ib	06:16:16.16	−21:22:09.8	±0″.2	NGC 2207 (4)	31.3	2011 Mar 10[d]	S	1800 s × 2	1″.1
2008bo	Ib	18:19:54.41	+74:34:21.0	±0″.2	NGC 6643 (2)	22.1	2010 Aug 1	S	1800 s × 1	0″.8
2009jf	Ib	23:04:52.98	+12:19:59.5	±0″.06	NGC 7479 (2)	33.9	2011 Sep 29	G	1800 s × 4	0″.5

Notes.
[a] Mean redshift-independent distance from NED (http://ned.ipac.caltech.edu).
[b] Hawaiian Standard Time (UTC−10).
[c] Instrument used: S = SNIFS, G = GMOS.
[d] The Great East Japan Earthquake occurred during the exposure of this object; the observation was conducted remotely from Tokyo, but fortunately, the earthquake did not introduce any effects on the observation and data.

photometric channel that is used to accurately place objects in the IFU. The positional accuracy with which the given (R.A., decl.) coordinates are placed on the IFU is around 0.2 arcsec. The scale and rotation of the SNIFS IFU is well measured thus should not produce much additional astrometric uncertainty. The spectrograph consists of two arms operating simultaneously to cover the whole optical wavelength range at $R \sim 1000$: the blue channel covers 3300–5200 Å and the red channel covers 5100–9700 Å. SNIFS is operated remotely with a fully dedicated data reduction pipeline. The final pipeline result is wavelength- and flux-calibrated (x, y, λ) data cubes. The description of the pipeline is similar to what is presented in Section 4 of Bacon et al. (2001) and is outlined briefly in Aldering et al. (2006).

Observations of the other four targets were carried out using the Gemini Multi-Object Spectrograph (GMOS) in IFU mode (Allington-Smith et al. 2002; Hook et al. 2004) with the 8.1 m Gemini North telescope at Mauna Kea (Program ID GN-2011B-C-6, via Subaru–Gemini Time Exchange Program). GMOS was used in one-slit mode, providing a $5'' \times 3''.5$ FoV sampled by the hexagonal lenslet array with one lenslet diameter of $0''.2$. We used the B600 grating centered at 5400 Å, and also took identical exposures with the grating centered at 5450 Å in order to perform spectral dithering to eliminate cosmic rays and cover the gaps of the three CCDs utilized by GMOS. This enables us to observe continuous spectra from 4000 Å to 6800 Å at $R \sim 1700$, thus covering and resolving prominent spectral lines such as Hα, Hβ, Hγ, Hδ, [O III] $\lambda\lambda4959, 5007$, [N II] $\lambda\lambda6548, 6583$, and [S II] $\lambda\lambda6716, 6731$. Subsequent data reduction was carried out using the Gemini package in IRAF.[10] The data were reduced to remove instrumental signatures and then calibrated in wavelength and flux to produce final (x, y, λ) data cubes.

Once the raw SNIFS and GMOS data were fully reduced into (x, y, λ) data cubes, object spectrum extraction and analysis were done using IRAF. The data cubes were treated as stacks of images taken at different wavelengths. The flux density of an object at each wavelength "slice" was extracted by performing aperture photometry (IRAF/*apphot*) on the object at each slice,

and arranging the values in the wavelength direction to produce a spectrum. The seeing FWHM was used as the radius of the circular aperture, or in some cases smaller apertures were used due to object proximity to the edge of the FoV. Sky in SNIFS data was estimated using an annular aperture around the object and was subtracted. Usually the annulus is larger than the field width; thus, effectively only a part of it was being used to measure the sky. GMOS is equipped with another IFU dedicated to simultaneous sky observation during the science exposures, and subtraction was done during the reduction process.

The positions of the objects in each SNIFS wavelength slice were traced, thus compensating for the differential atmospheric refraction (DAR) effect (Filippenko 1982). This demonstrates the advantage of using integral field spectroscopy (IFS) compared to conventional slit spectroscopy which is strongly affected by DAR, and with IFS the effects of DAR could be corrected a posteriori as has been shown by Arribas et al. (1999). The GMOS data set was corrected for DAR in the data cube stage by shifting each wavelength slice, and aperture photometry of individual slices was done with fixed aperture position for each object.

The final resulting spectra were then analyzed using IRAF/*splot*. Nebular emission lines were measured by fitting a Gaussian profile. To measure metallicity, only the nebular emission lines are needed thus the stellar continuum was removed prior to line measurement by fitting a polynomial function. Before measuring line EW, the continuum was normalized also by fitting with a polynomial. Metallicity in terms of oxygen abundance was derived using the O3N2 and N2 calibrations by Pettini & Pagel (2004, hereafter PP04). This method of metallicity determination uses intensity ratios of lines closely spaced in wavelength, and therefore is not sensitive to errors introduced by reddening and flux calibration.

Following PP04, we adopt 12+log (O/H) = 8.66 as the value of the solar oxygen abundance (Asplund et al. 2004). Hα and [N II] $\lambda6583$ were detected in all of the observed fields, thus enabling N2 determination while the Hβ and [O III] $\lambda5007$ detection required for O3N2 was less frequent. In cases where both O3N2 and N2 were detected we adopted the mean value as the metallicity, otherwise the N2 value was adopted. The errors quoted in metallicity in units of $Z_\odot$ are the bounds for the highest

---

[10] IRAF is distributed by the National Optical Astronomy Observatory, which is operated by the Association of Universities for Research in Astronomy, Inc., under cooperative agreement with the National Science Foundation.
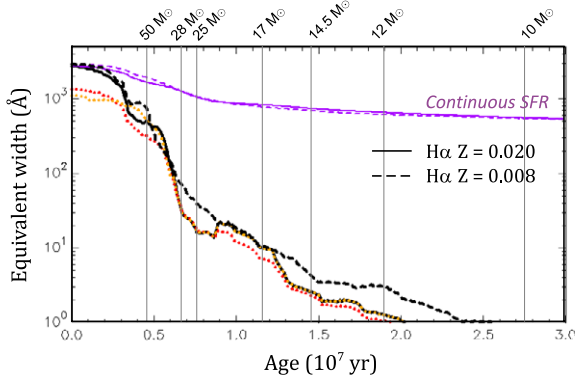
Figure 1. Time evolution of a Hα EW, Starburst99 SSP. The single-burst model is represented by the black line and continuous star formation by the purple line; both use a standard Salpeter IMF with $\alpha = 2.35$, $M_{up} = 100\,M_\odot$. Dotted lines represent single-burst solar-metallicity models with different IMFs: red is for $\alpha = 3.30$, $M_{up} = 100\,M_\odot$, and orange is for $\alpha = 2.35$, $M_{up} = 30\,M_\odot$. The lifetimes of single stars of different initial masses at solar metallicity according to Padova models are indicated with vertical gray lines.

(A color version of this figure is available in the online journal.)

and lowest values of 12+log(O/H) determined from O3N2 and N2. In cases where only N2 is available, we assign the error of 12+log(O/H) as ±0.18 dex, which is the 1σ uncertainty in PP04's N2 calibration determination. These were then converted into $Z_\odot$ metallicities to give the highest and lowest value bounds of metallicity.

Ages of the stellar populations were determined by comparing the observed Hα EW with the theoretical values provided by a simple stellar population (SSP) model, Starburst99 (Leitherer et al. 1999), for each appropriate metallicity. We assume an instantaneous burst stellar population with a continuous, standard Salpeter initial mass function (IMF; $\alpha = 2.35$). The evolution of Hα EW with SSP age is presented in Figure 1. The Hα EW of a stellar population with continuous star formation is also shown for comparison. The evolution of Hα is sensitive to the star formation history, while IMF variations have a less important effect especially at an SSP age older than ~4 Myr. The error of Hα EW was estimated from the signal-to-noise ratio of the spectral continuum around Hα. We expect the effect of dust absorption in Hα EW determination to be minimal due to the very small wavelength range used for EW measurement. The SSP age determined from Hα EW is adopted as the lifetime of the coeval progenitor star, and comparison with Padova stellar evolution models gives the estimated initial mass of a star with such a lifetime. We used models from Bressan et al. (1993) for solar metallicity ($Z = 0.02$), and Fagotto et al. (1994) for 0.4 solar metallicity ($Z = 0.008$). We defined the observed oxygen abundance of 0.7 (O/H)$_\odot$, corresponding to 12+log(O/H) = 8.50, as the dividing line between using the solar-metallicity model or the sub-solar one to determine stellar initial mass. These models extend from the zero-age main sequence to the onset of central carbon burning. This is considered representative of the stellar lifetime since the time elapsed from carbon burning to SN is only about a few hundred years, negligible compared to the $\sim 10^6$–10^7 yr lifetime of the star.

We compare the Starburst99 model of the Hα EW against GALEV (Anders & Fritze-v. Alvensleben 2003; Kotulla et al. 2009) to check for consistency and possible systematic effects. Both SSP models consider the contribution of stellar and nebular continuum to the output light, but GALEV includes nebular line emissions. As for the Hα EW value as a function of SSP age, Starburst99 provides the tabulation of the values while
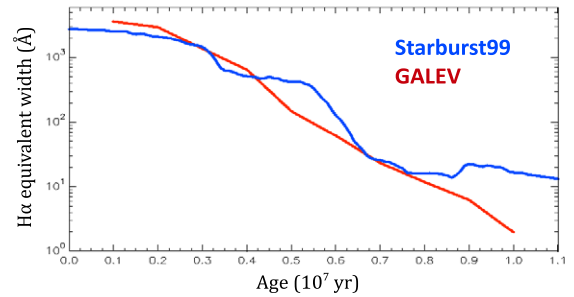
Figure 2. Comparison of the Hα EW evolution from different SSP models Starburst99 and GALEV.

(A color version of this figure is available in the online journal.)

GALEV does not. Therefore, individual spectra of GALEV SSP models of different ages were extracted and then Hα EWs were measured using IRAF/*splot* with the same procedure as the one applied to observational data. The result comparing the two different SSP models is presented in Figure 2. For both Starburst99 and GALEV we assume an instantaneous burst of a stellar population with a Salpeter IMF at solar metallicity, using the Geneva stellar library. From the plot it is evident that the Hα EW may differ by a factor of two or more between the two models. We attribute this difference to be partly because of the resolution difference of the model spectral energy distribution (SED). GALEV SEDs have a resolution of 20 Å at Hα, thus the neighboring nitrogen lines ([N II] λλ6548, 6583) were not resolved and hence contaminated the Hα in the EW measurement. However, this EW difference translates into only a small difference in age, on the order of 1–2 Myr. This, eventually, will lead to a difference of typically only about 20%–30% or lower in star initial mass, depending on the region of the age probed by the Hα EW. Therefore, we conclude that the selection of the SSP model does not introduce significant systematic effects on the final result of the progenitor star initial mass. In this case, Starburst99 was preferred over GALEV since it has better temporal resolution.

3. THE EXPLOSION SITES

3.1. SNe Ic Sites

3.1.1. SN 1964L Site

SN 1964L exploded in NGC 3938, a spiral galaxy hosting two other SNe (SNe II 1961U and 2005ay; see Paper II). This SN is poorly studied and no reference discussing the nature of the progenitor of this particular object was found in the literature. Blaylock et al. (2000) recovered the photographic spectra of the SN and classified it as Type Ic. We found that the cited position of SN 1964L is within 3 arcsec of a bright cluster in the host galaxy. Based on the measurements of the Palomar survey plates, the position was shown to be accurate to within 2″ by Porter (1993). SNIFS data show that this source exhibits a blue continuum with strong emission lines, typical of a young stellar population. Figure 3 shows the appearances of the explosion site on the IFU focal plane and the extracted spectrum of the host cluster. The measured metallicity is 1.09 solar. Measurement of the Hα EW shows that the cluster is very young, with a derived age of 3.3 Myr. The corresponding stellar initial mass of that age at solar metallicity is about 120 $M_\odot$.

3.1.2. SN 1994I Site

SN 1994I is one of the best-studied SNe Ic due to its location in M51, a very well observed nearby galaxy. It has often been
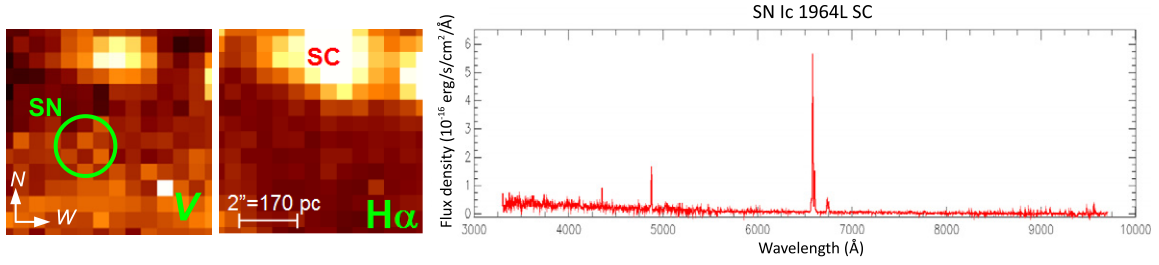
Figure 3. Left panel: SN 1964L site reconstructed IFU FoV. The SN position within a 1 arcsec error radius is indicated by a circle. An approximate linear scale corresponding to 2 arcsec is also indicated; this scale is calculated only from the host galaxy distance so does not take into account the projection effect and host galaxy inclination. "SC" indicates the host star cluster. Right panel: extracted spectrum of the star cluster.

(A color version of this figure is available in the online journal.)
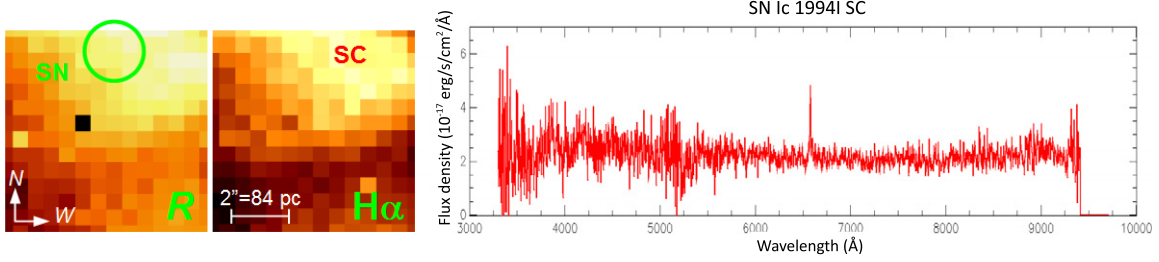
Figure 4. IFU FoV and extracted host cluster spectrum for the SN 1994I site. The red end of the spectrum is truncated due to DAR. Figure annotations are the same as in Figure 3.

(A color version of this figure is available in the online journal.)
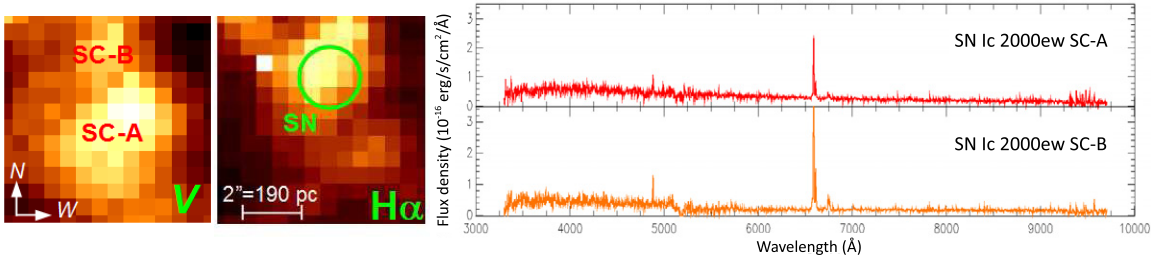
Figure 5. IFU FoV and extracted cluster spectra for the SN 2000ew site. Figure annotations are the same as in Figure 3.

(A color version of this figure is available in the online journal.)

referred to as the "standard" SN Ic although it also exhibited unusual behavior (e.g., Sauer et al. 2006). Nomoto et al. (1994) suggest that the progenitor of this SN is a 4.0 $M_\odot$ helium star in a binary system rather than a single WR star, which later evolved into a C+O star and eventually produced a SN Ic explosion. The main-sequence initial mass of this star was estimated to be 15 $M_\odot$. The position of this SN is accurate within $1''$, as estimated by van Dyk (1992) for SNe of that era and later confirmed by the late-time observations of Clocchiatti et al. (2008).

Our SNIFS result shows that the explosion site is rather diffuse; the host cluster does not stand out prominently over the stellar background (Figure 4). The extracted spectrum shows a faint continuum and a weak Hα line. Metallicity was derived as 0.83 solar from N2—this SN is the only SN Ic without an O3N2 determination in our sample since the Hβ and [O III] $\lambda 5007$ lines are not detected. The Hα EW corresponds to an age of 11.0 Myr. This age at solar metallicity corresponds to the lifetime of a 17.9 $M_\odot$ star, which is too low for a single WR progenitor but quite consistent with the binary model of Nomoto et al. (1994). This is possibly one of the first strong pieces of evidence of a binary progenitor channel in SN Ic production.

3.1.3. SN 2000ew Site

SN 2000ew exploded in NGC 3810 and is the first SN Ic with detected emission of near-infrared carbon monoxide (CO)

in the spectrum (Gerardy et al. 2002). Van Dyk et al. (2003) searched the progenitor star in the pre-explosion images but found none within their detection limit. Compared with *Hubble Space Telescope* (*HST*) images taken while the SN is still visible, the derived SN position is accurate to within $0''.7$. However, they discovered that luminous blue–yellow stars are present in the explosion site, within 1 arcsec of the SN position. The color–magnitude diagram suggests that the environment is very young, $\lesssim 6$ Myr old. Similarly, Maund & Smartt (2005) also failed to detect the progenitor star in pre-explosion images and derived an age estimate of the environment within 6 arcsec from the SN of ∼7 Myr, assuming twice solar metallicity. Maund & Smartt (2005) estimated a progenitor mass between 12 and 40 $M_\odot$ from the environment age.

Our SNIFS result shows that the cluster coincident with SN position, indicated as SC-B in Figure 5, is indeed very young, with an age of 5.8 Myr. This is consistent with the estimate of Van Dyk et al. (2003). The brighter neighboring cluster, SC-A, is slightly older, 6.3 Myr. Both clusters have similar metallicities of 1.15 and 1.05 solar, respectively. This onsite metallicity measurement is definitely more reliable compared to the twice-solar metallicity assumed in the previous studies. The corresponding main-sequence initial mass for a 5.8 Myr stellar population at solar metallicity is 33.9 $M_\odot$ while it is 29.5 $M_\odot$ for the 6.3 Myr population.
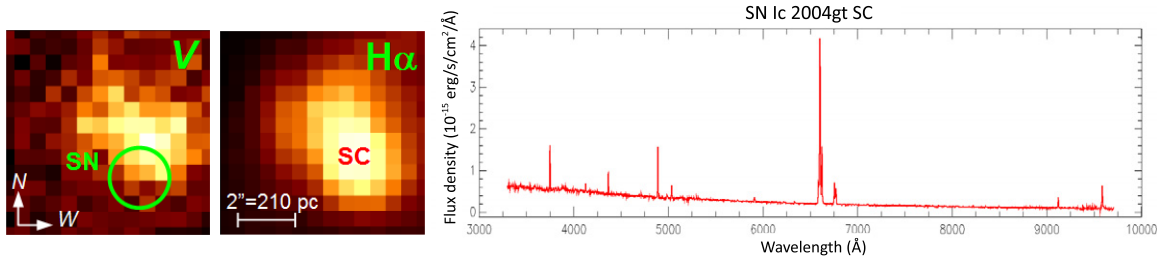
Figure 6. IFU FoV and extracted host cluster spectrum for the SN 2004gt site. Figure annotations are the same as in Figure 3.

(A color version of this figure is available in the online journal.)
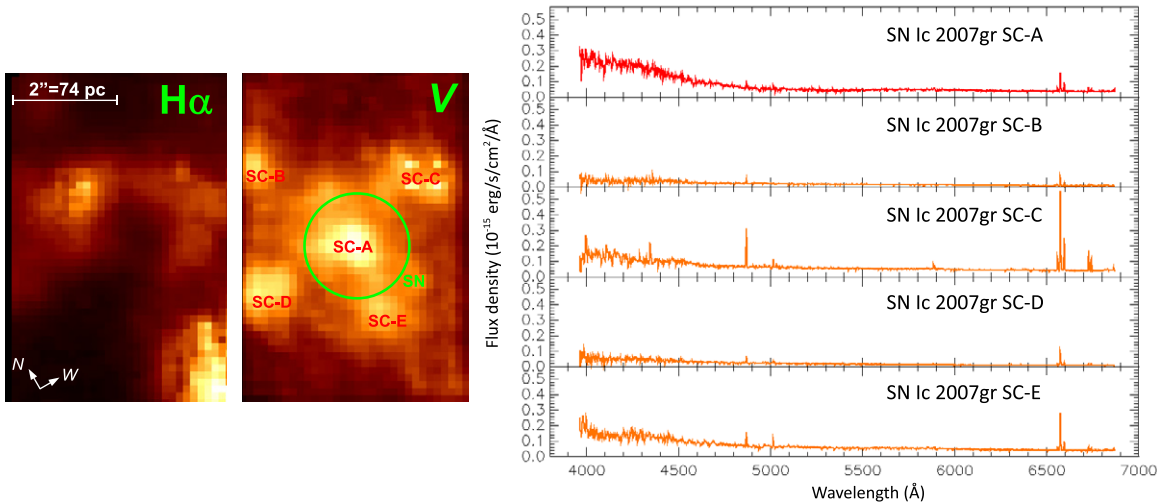
Figure 7. IFU FoV and extracted cluster spectra for the SN 2007gr site. The continuum image of the GMOS FoV was made by collapsing the data cube in the wavelength direction, approximately covering the *V* band. Figure annotations are the same as in Figure 3.

(A color version of this figure is available in the online journal.)

3.1.4. SN 2004gt Site

Gal-Yam et al. (2005), and Maund et al. (2005), reported their efforts at recovering the pre-explosion progenitor of SN 2004gt in the Antennae Galaxy, NGC 4038. However, the detection results were negative and only upper luminosity limits could be derived for the progenitor star (positional uncertainty 5 mas). Both investigations could not rule out a massive WR star progenitor, and also allow for a binary interaction scenario for producing the stripped-envelope progenitor star. The positional uncertainty of the SN in the *HST* images was estimated to be around 5 mas.

Our result with SNIFS shows that SN 2004gt exploded in a large star cluster complex (Figure 6), identified as Knot S by Whitmore et al. (2010). We derived the metallicity of Knot S as $12+\log(O/H) = 8.71$, or 1.12 solar, with an age of 5.78 Myr. This result is consistent with the Knot S mean age estimate of Whitmore et al. (2010) of 5.75 Myr. The age of 5.78 Myr corresponds to the lifetime of a star with an initial mass of $33.7\,M_\odot$ at solar metallicity. We also detect a WR star feature in the spectra at 4650 Å. A metallicity determination of the explosion site by Modjaz et al. (2011) gave $12+\log(O/H) = 8.70^{+0.00}_{-0.01}$ using the PP04 O3N2 scale. Our O3N2 determination yields a higher value, $12+\log(O/H) = 8.78$. The difference may have come from the different regions being observed, due to the different spectroscopy techniques (slit versus IFU). However, if the uncertainty in the PP04 O3N2 calibration of 0.14 dex is considered to be the error for both determinations, this difference is statistically insignificant, corresponding to only 0.4σ.

3.1.5. SN 2007gr Site

We used GMOS to observe the explosion site of SN 2007gr which exploded in the galaxy NGC 1058. Hunter et al. (2009) reported an extensive observation of the SN at optical and infrared wavelengths, covering more than 400 days. They showed that the photometric evolution of SN 2007gr is similar to SN 2002ap, an energetic Ic hypernova, but the spectra of the two SNe show marked differences. Tanaka et al. (2008) performed a spectropolarimetric observation of the SN and suggested that a bipolar explosion viewed slightly off-axis may best represent the explosion model of SN 2007gr. A study by Crockett et al. (2008b) using pre-explosion imaging data reported that the SN exploded very near ($\sim$7 pc) a point-like source in *HST* images, which they proposed as the compact host star cluster of the SN progenitor star. The positional uncertainty of the SN is about $0\rlap{.}''02$. Their determination of the compact cluster age using broadband photometry gives two solutions: 7 and 20–30 Myr assuming solar metallicity, corresponding to turnoff masses of 28 and 12–9 $M_\odot$, respectively.

A GMOS observation of the explosion site was seeing-limited at $0\rlap{.}''5$. Despite the excellent seeing condition, the compact clusters and bright individual stars comprising the OB association resolved in *HST* images could not be resolved and they appear collectively as bright knots in the IFU reconstructed images (Figure 7). We extracted the spectra of each of these five sources, designated SC-A through SC-E, including the central association where SN 2007gr exploded (SC-A). We derived the metallicity of SC-A as 1.12 solar, with an age of 7.8 Myr, quite consistent with the 7 Myr solution of Crockett et al. (2008b).
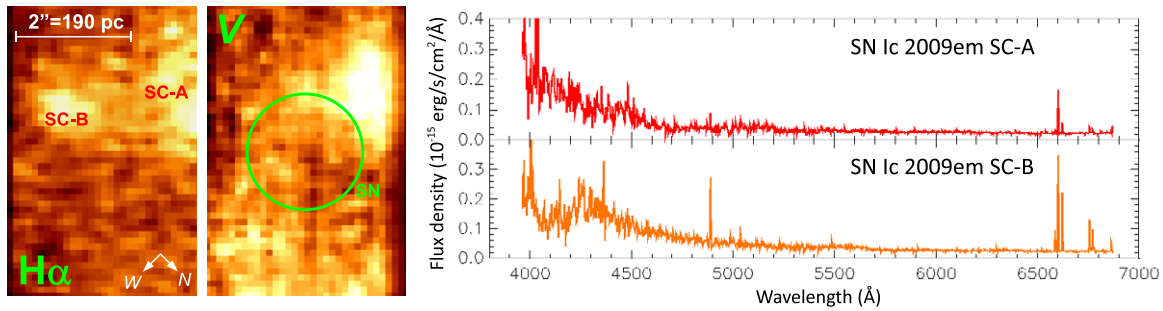
Figure 8. IFU FoV and extracted cluster spectra for the SN 2009em site. Figure annotations are the same as in Figure 3.
(A color version of this figure is available in the online journal.)
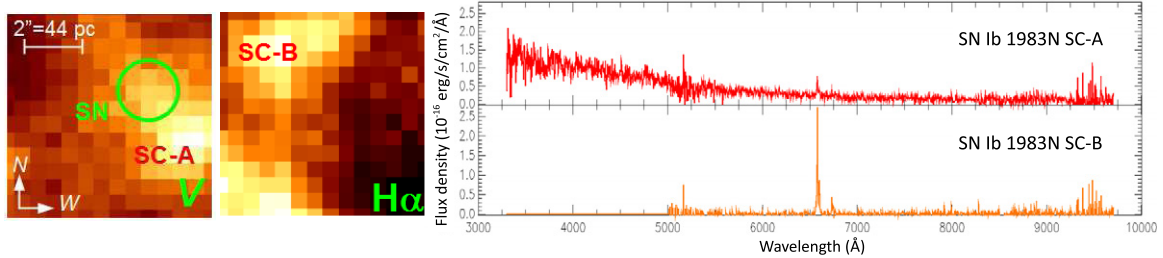
Figure 9. IFU FoV and extracted cluster spectra for the SN 1983N site. Figure annotations are the same as in Figure 3. The blue part of SC-B spectrum could not be extracted since it fell outside the FoV due to DAR.

(A color version of this figure is available in the online journal.)

This age corresponds to the lifetime of a 24.4 $M_\odot$ star at solar metallicity. Modjaz et al. (2011) measured the metallicity at the explosion site to be 12+log(O/H) = $8.64^{+0.07}_{-0.09}$ on the PP04 O3N2 scale. Our O3N2 determination yields 12+log(O/H) = 8.69, which is different from Modjaz et al.'s (2011) result only by 0.25σ—this is not significantly different.

Compared to other surrounding knots, SC-A appears to be older by about 1 Myr. All other knots—SC-B through SC-E—have ages between 6.4 and 6.8 Myr, which may suggest triggered star formation propagating inside-out from SC-A. If star formation in the outer clusters was triggered from SC-A, then the 1 Myr time difference and ~50 pc projected distance would correspond to a projected propagation velocity of ~50 km s^{-1}. The Hα map of the region shows a shell-like structure surrounding SC-A and coincident with the other four knots, leaving a depression in Hα intensity at the position of SC-A—further reinforcing this scenario. In any case, the ages of the other four knots correspond very well with the lifetimes of massive stars, around 28–29 $M_\odot$. Interestingly, SC-E shows relatively lower, sub-solar metallicity (0.85 $Z_\odot$) compared to other knots present at the site, which are super-solar (>1.1 $Z_\odot$).

3.1.6. SN 2009em Site

The Ic SN 2009em is not well studied. It was discovered by Monard (2009) about two months after maximum light as confirmed by Navasardyan & Benetti (2009) and also by Folatelli & Morrell (2009). The spectrum matches normal Type Ic events. There is no other information on this object available in the literature. We assign positional uncertainty of the SN as 1″, considering that it is a modern SN. The host galaxy NGC 157 is a grand-design Sc spiral, harboring no other SN to date except 2009em.

With GMOS we observed the explosion site and detected two clusters (Figure 8). The more prominent cluster, SC-A, exhibits a sub-solar metallicity of 0.76 $Z_\odot$, with an age of 6.8 Myr. The neighboring fainter cluster SC-B is barely detected

in continuum images but stands out in Hα. It has nearly twice the metallicity of SC-A, 1.45 solar. The age of this cluster was derived as 6.3 Myr. The significant difference between the two clusters' metallicities illustrates the importance of measuring the metallicity of explosion sites with fine spatial resolution. The SN itself exploded at about the same distance from both clusters, but we assigned SC-A as the host cluster since it is the brighter one and thus more likely to host more progenitor candidates. The ages of the clusters correspond to the lifetimes of 27.7 and 29.5 $M_\odot$ stars, for SC-A and SC-B, respectively.

3.2. SNe Ib Sites

3.2.1. SN 1983N Site

SN 1983N exploded in a nearby large spiral galaxy, M83 (NGC 5236). This SN was observed extensively (e.g., Gaskell et al. 1986; Weiler et al. 1986; Clocchiatti et al. 1996) and has been suggested to be the prototypical SNe Ib along with SN 1984L (Porter & Filippenko 1987). Sramek et al. (1984) reported the first radio detection of a type-I SN: SN 1983N. Clocchiatti et al. (1996) reported that their astrometry of the SN position is accurate to within ~0″.6.

Using SNIFS we discovered that the explosion site of the SN is quite complex, with three detected objects within the IFU FoV. In the continuum a prominent cluster was detected, but this cluster is overshadowed in Hα by two bright nearby H II regions (see Figure 9). We extracted the spectra of the SC-A cluster and the H II region northeast of it (SC-B), but failed to do so for the H II region southeast of the cluster since it is situated at the edge of the FoV. It is likely that this third cluster is similar in age to SC-B considering its detectability in Hα and non-detection in continuum images. The cluster SC-A was found to be 7.2 Myr old with 1.02 times solar metallicity, while the H II region SC-B has an age of 2.6 Myr with 0.89 solar metallicity. The age of SC-A corresponds to the lifetime of a 26.4 $M_\odot$ star, while the SC-B age is considered too young to even produce an SN.
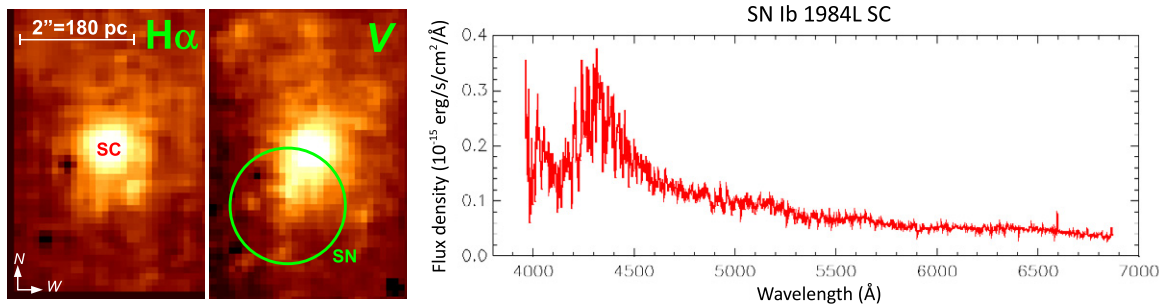
Figure 10. IFU FoV and extracted host cluster spectrum for the SN 1984L site. Figure annotations are the same as in Figure 3.
(A color version of this figure is available in the online journal.)
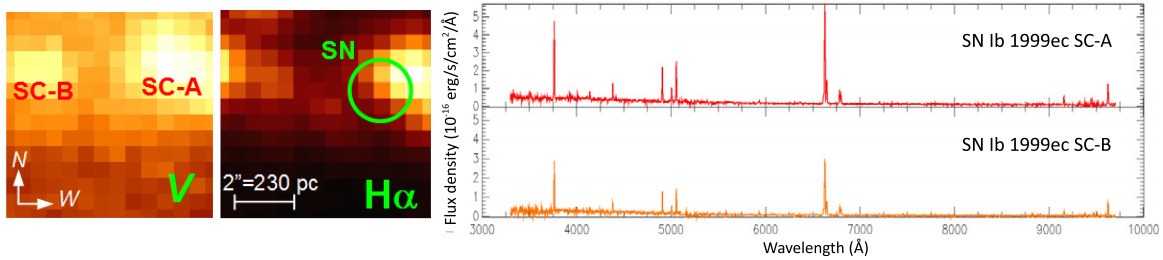
Figure 11. IFU FoV and extracted cluster spectra for the SN 1999ec site. Figure annotations are the same as in Figure 3.
(A color version of this figure is available in the online journal.)

3.2.2. SN 1984L Site

SN 1984L exploded in NGC 991, a low surface brightness spiral galaxy. Schlegel & Kirshner (1989) presented late-time photometry and spectroscopy of the SN, and suggested that it originated from a roughly $20\,M_\odot$ star. Later, Swartz & Wheeler (1991) derived an ejecta mass of more than $10\,M_\odot$, which they inferred to be the result of an explosion of a $\gtrsim 30\,M_\odot$ star. Baron et al. (1993) put forward the problem of reconciling the early-time light curve with the spectra of the SN, for which they proposed a solution by suggesting a scenario in which the explosion of a very massive star ($\sim 50\,M_\odot$ of helium with 2×10^{52} erg kinetic energy) produced a massive black hole. The coordinates given by Schlegel & Kirshner (1989) differ by about $0\farcs3$ compared to those of Weiler et al. (1986). This value is used as the positional uncertainty of SN 1984L.

Our GMOS observation of the explosion site shows that the host star cluster of SN 1984L does not exhibit strong emission lines in its spectrum, indicating intermediate age (Figure 10). We measured the metallicity to be 0.45 solar, the lowest in our sample. The Hα emission EW is small, giving an age estimate of 18.0 Myr, which corresponds to the lifetime of a $13.5\,M_\odot$ star. This result is inconsistent with previous studies, suggesting a high-mass ($\gtrsim 20\,M_\odot$) progenitor, but is intriguing since the derived mass of $13.5\,M_\odot$ lies well below the currently accepted WR star mass limit and within the range of SN II-P progenitors. With such low metallicity, it is even more difficult to remove the hydrogen envelope of a single star via the stellar wind mechanism, and as a result the minimum mass needed for a star to become a WR star increases. Thus, this is a strong indication that the SN 1984L progenitor may have lost its envelope in a close binary system.

3.2.3. SN 1999ec Site

The SN Ib 1999ec exploded in the interacting spiral galaxy, NGC 2207. Currently, there have been four recorded SNe that have occurred in this galaxy (SNe 1975A, 1999ec, 2003H,

2013ai). Van Dyk et al. (2003) searched for the progenitor star in pre-explosion images but found no convincing candidate. Their *HST* images show that the SN occurred in an environment of blue, apparently young stars and clusters. The SN position uncertainty was $\pm 0\farcs2$.

With SNIFS we detect two large clusters in the SN vicinity (Figure 11). Both clusters have similar spectra and are of similar metallicity, with SC-A being 0.71 solar value and SC-B of 0.74 solar. Both are also similar in derived age, with SC-A being 5.3 Myr and SC-B being 5.1 Myr. These age estimates at solar metallicity correspond to the lifetimes of 38.0 and $41.6\,M_\odot$ stars, respectively. The derived initial mass is high, even compared to the majority of SN Ic progenitors.

3.2.4. SN 2008bo Site

SN 2008bo exploded in a spiral host, NGC 6643. This SN has been detected in X-ray (Immler et al. 2008; Immler & Brown 2008) and radio (Stockdale et al. 2008) wavelengths. The Asiago database assigned Type Ib for this SN; Navasardyan et al. (2008) reported that the spectrum shows the characteristics of a stripped-envelope event but with deep Hα absorption. This resembles the spectrum of SN 2008ax, an SN IIb, which shows spectral evolution from Type II to Ib. There is no other useful discussion about the physical nature of the object in the literature. Stockdale et al. (2008) reported that the radio position of this SN agrees well ($\sim 0\farcs2$) with the optical position. Thus, we assign $0\farcs2$ as the positional uncertainty of this SN.

We observed the explosion site using SNIFS and extracted the spectra of two clusters apparent at the site (Figure 12). A prominent cluster, SC-A, appears in all wavelengths while in Hα we detect a faint secondary cluster, SC-B, and some other fainter structures in the FoV. We performed an additional imaging observation of the SN 2008bo site using the OPTIC camera at UH88 (Howell & Tonry 2003) in 2011. However, the surrounding fainter structures are not visible in our broadband images. From SNIFS data SC-A was found to be 13.5 Myr old
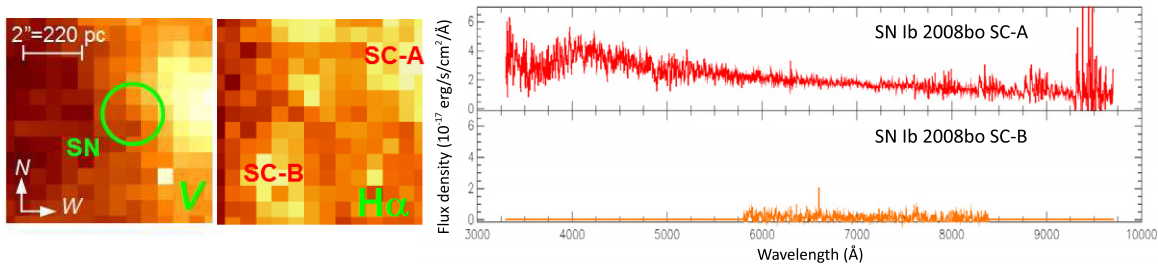
Figure 12. IFU FoV and extracted cluster spectra for the SN 2008bo site. Figure annotations are the same as in Figure 3. Only a part of the SC-B spectrum could be recovered due to DAR effects.

(A color version of this figure is available in the online journal.)
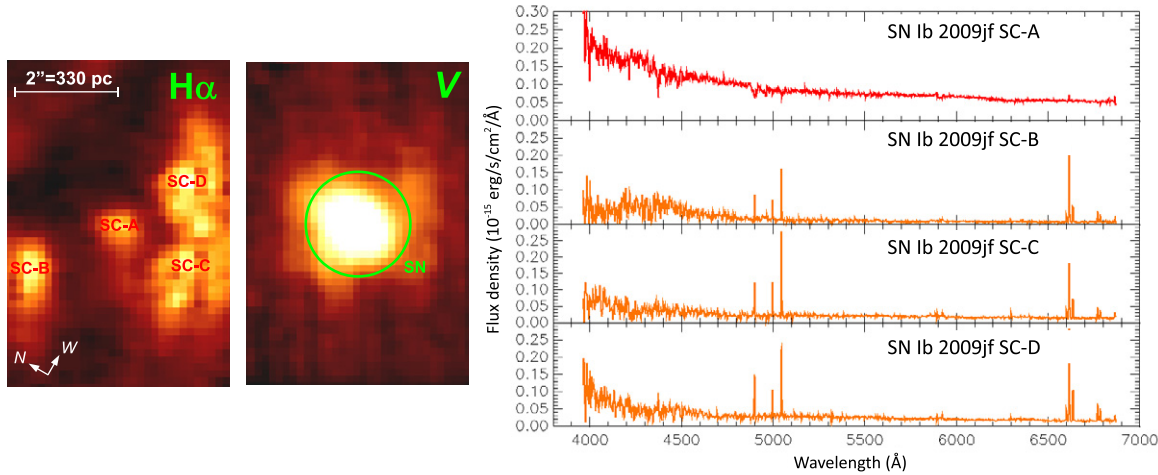
Figure 13. IFU FoV and extracted cluster spectra for the SN 2009jf site. Figure annotations are the same as in Figure 3.

(A color version of this figure is available in the online journal.)

with 1.20 solar metallicity. We only managed to extract a part of the spectrum of SC-B but nevertheless recovered the Hα region and derived an age via its EW, which is 6.4 Myr. The metallicity of SC-B is derived as 0.85 solar. The 13.5 Myr age corresponds to a star with an initial mass of 14.9 $M_\odot$, while 6.4 Myr corresponds to 29.3 $M_\odot$. The 14.9 $M_\odot$ derived mass is too small for a star to produce a WR star that may later explode as an SN Ib, thus it is likely that SN 2008bo also may have been produced by a progenitor in a binary system.

3.2.5. SN 2009jf Site

SN 2009jf exploded in one of the two prominent spiral arms of the barred spiral galaxy NGC 7479. It was an energetic slow-evolving SN, indicating massive ejecta. Sahu et al. (2011) presented nine months of optical photometry and spectroscopy monitoring of this SN and suggested that the main-sequence mass of the progenitor is $\gtrsim$20–25 $M_\odot$ estimated from the ejecta mass. Further, Valenti et al. (2011) also reported their one-year monitoring of SN 2009jf and similarly concluded that the progenitor mass range is within 25–30 $M_\odot$. Their positional uncertainty of the SN is on the order of 0″06.

We observed the explosion site of SN 2009jf using GMOS two years after the discovery. The continuum IFU reconstructed image shows only one prominent source in the field (Figure 13), which is the blended source A+B in Valenti et al. (2011). We assigned this blended source the designation SC-A star cluster. Making use of the capability of IFU we reconstructed Hα image of the field, and found that a clumpy shell-like structure of ionized gas is present around SC-A. We assigned identifications

SC-B, SC-C, and SC-D to these clumps. We found that the metallicity of this complex is below solar, with SC-A being 0.78 solar value and SC-B, C, D within 0.63–0.81 solar. The N2 metallicity of SC-A in 12+log(O/H) equals 8.55 dex, and agrees exactly with the explosion site metallicity estimate of Sanders et al. (2012), using slit spectroscopy of 0″7 slit width. However, they do not mention the aperture size for spectrum extraction or the seeing size during the observation. Sanders et al. (2012) determined the age of the explosion site from Hβ EW to be 9.0 Myr. The age of SC-A from our determination is quite old, 18.2 Myr, which corresponds to the lifetime of a 12.4 $M_\odot$ star. The surrounding clusters are significantly younger, between 6.0 and 6.4 Myr. These morphological characteristics are similar to what we found at the SN 2007gr explosion site, where the central host cluster in the complex is older than the surroundings thus suggesting inside-out star formation activity. This formation scenario has been observed elsewhere (e.g., Adamo et al. 2012), thus suggesting that triggered star formation may not be uncommon in star formation complexes. Assuming the outer clusters' formation was triggered by SC-A, the projected outward velocity of star formation propagation in this complex is ~300 pc per 12 Myr, or around 25 km s^{-1}. This is about half the projected velocity we inferred for the SN 2007gr site.

If the progenitor of SN 2009jf indeed originated in SC-A, this would be a third example after SN 1984L and SN 2008bo of a low-mass SN progenitor produced by a binary channel. In contrast, the surrounding environment age is consistent with the lifetime of stars with masses around 30 $M_\odot$. We note that the progenitor mass inferred from SN properties is more consistent with the outer environment age rather than the stellar

Table 2
Results for SN Ic Sites

SN Site	Object	Offset/″[a] (pc)	(O3N2)	(N2)	12+log(O/H)	Z ($Z_\odot$)	Hα EW (Å)	Age (Myr)	M ($M_\odot$)
1964L	SC*	2.6 (220)	8.83	8.57	8.70	$1.09^{+0.39}_{-0.27}$	939.10 ± 84.52	$3.28^{+0.04}_{-0.04}$	120^{-10}_{+1}
1994I	SC*	2.6 (110)	...	8.58	8.58	$0.83^{+0.43}_{-0.28}$	13.34 ± 1.87	$11.0^{+0.25}_{-0.75}$	$17.9^{-0.4}_{+0.8}$
2000ew	SC-A	2.3 (220)	8.77	8.58	8.68	$1.05^{+0.23}_{-0.22}$	68.18 ± 8.18	$6.31^{+0.04}_{-0.04}$	$29.5^{-0.2}_{+0.1}$
2000ew	SC-B*	1.2 (110)	8.85	8.59	8.72	$1.15^{+0.40}_{-0.30}$	221.10 ± 35.38	$5.75^{+0.09}_{-0.09}$	$33.9^{-0.8}_{+1.0}$
2004gt	SC*	1.3 (140)	8.78	8.64	8.71	$1.12^{+0.20}_{-0.17}$	209.60 ± 10.48	$5.78^{+0.03}_{-0.03}$	$33.7^{-0.3}_{+0.2}$
2007gr	SC-A*	0.0 (0)	8.69	8.72	8.71	$1.12^{+0.03}_{-0.05}$	15.57 ± 0.96	$7.84^{+0.75}_{-0.25}$	$24.4^{-2.5}_{+0.8}$
2007gr	SC-B	1.4 (52)	8.96	8.63	8.80	$1.35^{+0.64}_{-0.42}$	33.03 ± 3.30	$6.66^{+0.06}_{-0.05}$	$28.3^{-0.2}_{+0.1}$
2007gr	SC-C	1.1 (41)	8.82	8.68	8.75	$1.20^{+0.25}_{-0.20}$	59.62 ± 2.47	$6.36^{+0.01}_{-0.02}$	$29.3^{-0.1}_{+0.1}$
2007gr	SC-D	1.6 (59)	8.99	8.58	8.79	$1.35^{+0.79}_{-0.52}$	50.26 ± 5.03	$6.42^{+0.06}_{-0.04}$	$29.1^{-0.2}_{+0.2}$
2007gr	SC-E	1.0 (37)	8.65	8.54	8.60	$0.85^{-0.14}_{-0.09}$	27.95 ± 1.39	$6.78^{+0.08}_{-0.05}$	$27.9^{-0.3}_{+0.2}$
2009em	SC-A*	1.1 (100)	8.57	8.51	8.54	$0.76^{+0.05}_{-0.05}$	26.88 ± 2.69	$6.84^{+0.30}_{-0.09}$	$27.7^{-1.0}_{+0.4}$
2009em	SC-B	1.0 (94)	8.85	8.78	8.82	$1.45^{+0.10}_{-0.13}$	68.76 ± 5.09	$6.31^{+0.02}_{-0.03}$	$29.5^{-0.1}_{+0.1}$

Notes.
[a] Offset between SN and approximate cluster center.
* SN parent cluster.

Table 3
Results for SN Ib Sites

SN Site	Object	Offset/″[a] (pc)	(O3N2)	(N2)	12+log(O/H)	Z ($Z_\odot$)	Hα EW (Å)	Age (Myr)	M ($M_\odot$)
1983N	SC-A*	2.6 (57)	...	8.67	8.67	$1.02^{+0.53}_{-0.34}$	23.32 ± 4.19	$7.22^{+0.27}_{-0.42}$	$26.4^{-0.8}_{+1.4}$
1983N	SC-B	3.0 (66)	...	8.61	8.61	$0.89^{+0.46}_{-0.30}$	1693 ± 728	$2.62^{+0.65}_{-1.26}$	...
1984L	SC*	1.6 (150)	...	8.31	8.31	$0.45^{+0.13}_{-0.16}$	2.93 ± 0.49	$18.0^{+2.18}_{-2.21}$	$13.5^{-0.9}_{+1.1}$
1999ec	SC-A*	0.8 (90)	8.49	8.53	8.51	$0.71^{+0.30}_{-0.30}$	384.50 ± 46.14	$5.34^{+0.15}_{-0.35}$	$38.0^{-1.5}_{+5.0}$
1999ec	SC-B	3.3 (370)	8.51	8.55	8.53	$0.74^{+0.04}_{-0.02}$	424.10 ± 72.09	$5.06^{+0.40}_{-0.71}$	$41.6^{-4.8}_{+14.2}$
2008bo	SC-A*	3.1 (330)	...	8.74	8.74	$1.20^{+0.62}_{-0.41}$	3.13 ± 0.53	$13.5^{+1.03}_{-0.40}$	$14.9^{-0.5}_{+0.4}$
2008bo	SC-B	3.5 (380)	...	8.59	8.59	$0.85^{+0.44}_{-0.29}$	56.37 ± 48.48	$6.37^{+5.92}_{-0.24}$	$29.3^{-13.0}_{+0.9}$
2009jf	SC-A*	0.0 (0)	...	8.55	8.55	$0.78^{+0.39}_{-0.27}$	1.38 ± 0.12	$18.2^{+0.77}_{-0.52}$	$12.4^{-0.5}_{+0.3}$
2009jf	SC-B	1.4 (230)	8.42	8.53	8.48	$0.66^{+0.08}_{-0.08}$	140.6 ± 23.90	$6.02^{+0.16}_{-0.16}$	$34.7^{-0.9}_{+1.2}$
2009jf	SC-C	1.0 (160)	8.39	8.52	8.46	$0.63^{+0.09}_{-0.09}$	88.71 ± 9.76	$6.36^{+0.13}_{-0.08}$	$32.2^{-1.0}_{+0.6}$
2009jf	SC-D	1.2 (200)	8.50	8.63	8.57	$0.81^{+0.12}_{-0.12}$	80.36 ± 9.64	$6.25^{+0.04}_{-0.05}$	$29.7^{-0.2}_{+0.1}$

Notes.
[a] Offset between SN and approximate cluster center.
* SN parent cluster.

association closest with the SN position. Valenti et al. (2011) found that the color of their source A is consistent with a stellar population containing stars with the maximum stellar mass of 8–25 $M_\odot$, while source B is redder thus presumably older. This is not inconsistent with our findings which yield a progenitor mass of about 12 $M_\odot$. However, it is possible that the star formation history in the immediate vicinity of SN 2009jf is not instantaneous, and the progenitor star was born from a younger burst compared to the dominant older surrounding population.

4. DISCUSSIONS

It is very important to determine the metallicity and age of the explosion sites of SNe Ib/Ic to characterize their progenitor stars. Metallicity-driven wind is one widely accepted scenario to remove the star's hydrogen envelope and produce a stripped SN. Our results show that even at the SN explosion site metallicity variations may be present from place to place, thus emphasizing the importance of measuring local metallicity directly with the highest spatial resolution possible and discouraging metallicity determinations using proxies. The results are presented in Tables 2 and 3.

Averaging metallicities of all the 12 objects present at each explosion site, we found a mean metallicity for the sample of SN Ic sites of 1.11 ± 0.22 (rms; standard error of the mean/SEM = $\sigma/\sqrt{N} = \pm 0.06$) $Z_\odot$, while this value is reduced to 1.01 ± 0.17 (SEM = ± 0.08) $Z_\odot$ if only the SN parent clusters are considered. For the case of SN Ib sites the mean metallicity value is 0.79 ± 0.20 (SEM = ± 0.06) $Z_\odot$, and 0.83 ± 0.29 (SEM = ± 0.13) $Z_\odot$ for SN Ib host clusters only. Notwithstanding the somewhat small number of samples (6 SN Ic sites, 12 clusters; 5 SN Ib sites, 11 clusters), this immediately suggests that SNe Ic are produced in higher-metallicity environments than SNe Ib. The statistical significance of the difference between SN Ic and Ib host clusters' metallicities determined by the t-test is 1.2σ, while it is 3.7σ if we consider the site metallicities.

Modjaz et al. (2011) argued that SNe Ic and Ib explode in different metallicity environments with a difference of

0.2 dex in 12+log(O/H), with a total sample of $N = 35$. Their Kolmogorov–Smirnov (K-S) test p-value of the null hypothesis that both SN types came from the same population yields 1%. Converting our solar-unit metallicity values of the host clusters back into the 12+log(O/H) scale, we found a 0.08 dex difference between SN Ic and Ib explosion sites. The K-S test p-value for our two samples is 59%, which could not rule out the possibility that both samples are from the same population; however, this might not be very meaningful considering the small number statistics. For comparison, other studies by Leloudas et al. (2011, $N = 20$) and Sanders et al. (2012, $N = 33$) also suggest higher metallicity for Ic (albeit not statistically significant), while Anderson et al. (2010) found no difference between Ib and Ic metallicities ($N = 24$). The sample of Sanders et al. (2012) was drawn from untargeted SN surveys, thus is likely to be less biased toward massive, high-metallicity host galaxies compared to a sample drawn from targeted SN surveys. Our result ($N = 11$) of 1.2σ significance suggests that, on average, SNe Ic are more metal-rich compared to SNe Ib, but not statistically significant. Therefore, it is closer to the conclusion of Leloudas et al. (2011) who also suggested that SNe Ic are more metal-rich compared to SNe Ib, by 0.08 dex.

We note one interesting fact that for SN Ic sites the metallicity derived from the O3N2 index is almost always (10 out of 11) higher than from the N2 index (3.7σ significance), while it is the opposite for SN Ib sites (2.7σ significance). Consistently for both SN Ic and Ib sites the measured metallicity is always higher for SN Ic sites in either the O3N2 or N2 scale. The high O3N2 metallicity may be indicative of N/O enhancement (Pérez-Montero & Contini 2009). This behavior has been observed in galaxies with high O3N2 metallicity as reported by Berg et al. (2011), and interpreted as galaxies evolving past the WR galaxy phase as WR stars may elevate the observed N/O ratio.

The age of the SN explosion site provides a clue to the likely mass of the progenitor star. We averaged the age of all detected clusters in our SN sites and found that SN Ic sites have a younger mean age than SN Ib sites, 6.6 ± 1.7 (SEM = ± 0.5) Myr compared to 8.6 ± 5.3 (SEM = ± 1.6) Myr. This trend is also present when comparing the ages of the host clusters, with SN Ic hosts averaging 6.7 ± 2.6 (SEM = ± 1.1) Myr while for SN Ib hosts the age is significantly higher, 12.4 ± 5.9 (SEM = ± 2.6) Myr. This result shows that it is likely that SNe Ic resulted from higher-mass progenitors than SNe Ib (2.0σ significance). Considering the results for individual objects, we also suggest that some SN Ib/Ic progenitors may have originated from close binary systems due to the derived old age of the host cluster. SN 1994I is one example of a SN Ic with a derived old parent cluster age, or low-mass progenitor. The derived age of 10.9 Myr corresponds to the lifetime of a 17.9 $M_\odot$ single star, which is not massive enough to evolve into the stripped-envelope WR star thought necessary to produce a SN Ic. Therefore, one likely scenario is that this SN was the explosion of a star in a binary system whose hydrogen envelope has been removed by binary interactions. For SNe Ib in our sample we found that this scenario may be applicable to SNe 1984L, 2008bo, and 2009jf. It is also interesting to note that the binary scenario is significantly more prevalent in our SNe Ib samples (three out of five SNe) compared to SNe Ic (one out of six SNe), but further investigation with more samples is necessary to confirm this indication firmly.

It is interesting to note that SNe IIb, whose spectral evolution showed transition from Type II to Type Ib, already show evidence that points to a star in a binary system as the progenitor.
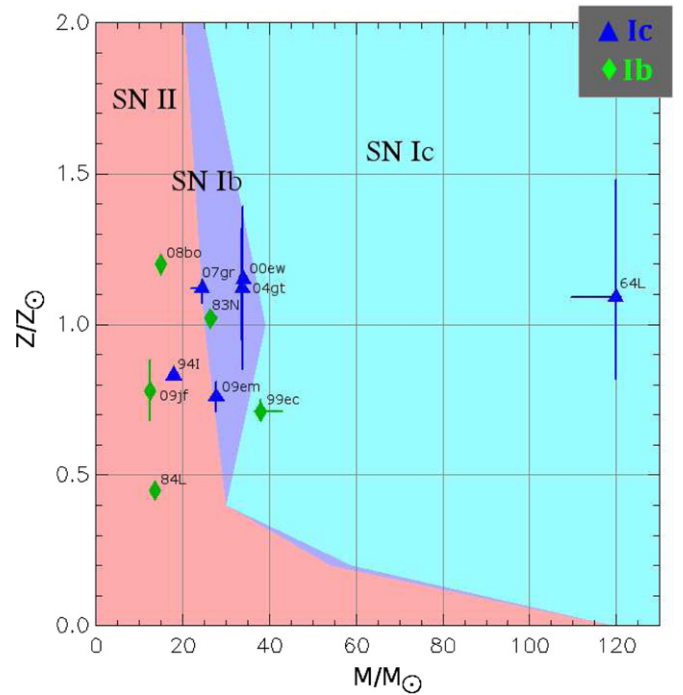
Figure 14. SN Ib/Ic progenitors overplotted on mass–metallicity space; Ic progenitors are indicated with purple triangles and Ib progenitors are indicated with green diamonds. Theoretical predictions of progenitors of each SN type by Georgy et al. (2009) are drawn as colored regions.

(A color version of this figure is available in the online journal.)

Aldering et al. (1994) showed that the SED of the SN 1993J progenitor could not be fit with a single star SED; further, Maund et al. (2004) reported the unambiguous detection of the companion star with a post-explosion observation. An indication of binarity was also found in recent IIb events: SN 2008ax (Crockett et al. 2008a) and SN 2011dh (Bersten et al. 2012). Based on the similarities, it is possible that both SNe IIb and Ib have similar binary progenitors.

With the information on SN host cluster age and metallicity, we derive the maximum mass of the stars still present in the cluster. As the most massive stars die first, any of the remaining stars would not exceed the mass of the SN progenitor exploded just recently. The age of the cluster is equal to the lifetime of the SN progenitor, and since the lifetime of a single star is mainly governed by its initial mass, the lifetime of the SN progenitor could be used to estimate its initial mass. With this method we determined the main-sequence mass of the SN progenitors in our sample by comparing to Padova stellar evolution models, adopting the metallicity of the parent cluster. We used the models by Bressan et al. (1993) for solar metallicity and Fagotto et al. (1994) for 0.4 solar metallicity. The resulting mass along with metallicity information for each SN progenitor is plotted on mass–metallicity space in Figure 14. Theoretical predictions of SN progenitors by Georgy et al. (2009) are overlaid to make the comparison readily available. It is immediately apparent that the theoretical models and observational data points do not agree very well—only one occurrence of observational data falls into the right theoretical prediction for each Ib/Ic type (SNe 1983N and 1964L). In spite of this, we argue that the relative comparison of the masses of progenitor stars of different SN types (i.e., Ib versus Ic) should be robust regardless of the stellar evolution model used. We also

Table 4
Mass and Age of SN Ib/Ic Progenitors from This Work, Compared with Other Determinations

SN	Mass (This Work)	Age (This Work)	Mass (Ref.)	Age (Ref.)	Method (Ref.)	Reference
Ic 1964L	120 $M_\odot$	3.28 Myr	. . .	. . .	. . .	. . .
Ic 1994I	17.9 $M_\odot$	. . .	15 $M_\odot$	. . .	SN properties	Nomoto et al. (1994)
Ic 2000ew	. . .	5.75 Myr	. . .	$\lesssim$6 Myr	Environment CMD	Van Dyk et al. (2003)
	33.9 $M_\odot$	. . .	12–40 $M_\odot$	. . .	Non-detection	Maund & Smartt (2005)
Ic 2004gt	. . .	5.78 Myr	. . .	5.75 Myr	SC color	Whitmore et al. (2010)
	33.7 $M_\odot$	. . .	$\gtrsim$40 $M_\odot$, or low-mass binary	. . .	Non-detection	Maund et al. (2005), Gal-Yam et al. (2005)
Ic 2007gr	24.4 $M_\odot$	7.84 Myr	28 or 12–9 $M_\odot$	7 or 20–30 Myr	SC color	Crockett et al. (2008b)
Ic 2009em	27.7 $M_\odot$	6.84 Myr	. . .	. . .	. . .	. . .
Ib 1983N	26.4 $M_\odot$	7.22 Myr	. . .	. . .	. . .	. . .
Ib 1984L	13.5 $M_\odot$	18.0 Myr	20 $M_\odot$	. . .	SN properties	Schlegel & Kirshner (1989)
			$\gtrsim$30 $M_\odot$	. . .	SN properties	Swartz & Wheeler (1991)
			$\gtrsim$50 $M_\odot$	. . .	SN properties	Baron et al. (1993)
Ib 1999ec	38.0 $M_\odot$	5.34 Myr	$M_V \gtrsim -8.7$	. . .	Non-detection	Van Dyk et al. (2003)
Ib 2008bo	14.9 $M_\odot$	13.5 Myr	. . .	. . .	. . .	. . .
Ib 2009jf	. . .	6–18 Myr	. . .	9.0 Myr	Site Hβ EW	Sanders et al. (2012)
	12.4–34.7 $M_\odot$	. . .	$\gtrsim$20–25 $M_\odot$	. . .	SN properties	Sahu et al. (2011)
	12.4–34.7 $M_\odot$	. . .	25–30 $M_\odot$	. . .	SN properties	Valenti et al. (2011)
	12.4–34.7 $M_\odot$	. . .	$\lesssim$8–25 $M_\odot$	. . .	SC color	Valenti et al. (2011)

Note. CMD: color–magnitude diagram; SC: star cluster.

compare our results for progenitor mass and local environment age with other observational results using different methods, summarized in Table 4. In general, our results do not contradict the findings of other studies, except probably for SN 1984L. This provides a strong confirmation of the validity of our method. However, we note that there is always the probability that we are suffering from projection effects which may cause an apparent association between the SN and an otherwise unrelated stellar population, resulting in a chance superposition. This issue is further addressed in Paper II, resulting in a 50% chance superposition estimate. Nevertheless, our method offers the current best determination of SN progenitor age and metallicity from the SN local environment. The median distance of objects in this study is ~15 Mpc (1″ corresponds to 70 pc), or redshift 0.0035 (for $H_0 = 70$ km s^{-1} Mpc^{-1}), the smallest compared to other similar studies. For example, the median redshift (distance) of objects in Anderson et al. (2010) is 0.005 (21 Mpc), 0.017 (72 Mpc) in Modjaz et al. (2011), 0.022 (94 Mpc) in Leloudas et al. (2011), and 0.036 (154 Mpc) in Sanders et al. (2012) (Table 8 of Sanders et al. 2012).

In this work we suggest that SNe Ic originate from more massive progenitors than SNe Ib, in agreement with Smith et al. (2011). The progenitor mass of SN Ic averages 42.9 ± 38.2 $M_\odot$, while for SN Ib the average progenitor mass is 21.0 ± 11.0 $M_\odot$. The high O3N2 metallicity of SN Ic sites supports this conclusion that SN Ic progenitors have mass within the WR star range. We note that the large deviation in SN Ic average progenitor mass is caused by the very high determined mass of SN 1964L, ~120 $M_\odot$. If we omit this one SN the average progenitor mass for SN Ic is reduced to 27.5 ± 6.7 $M_\odot$—still higher than the SN Ib progenitor average and consistent with WR star mass. The statistical significance of the Ib and Ic progenitor mass difference is 1.3σ, and the inclusion of SN 1964L will slightly reduce it to 1.1σ. Our results also show some examples where the progenitor may have originated from close binary systems, considering the old age of the parent stellar population. This is consistent with the findings of Leloudas et al. (2011), which suggest that both single or binary progenitor scenarios are at work for SN Ib/Ic production. Smith et al. (2011) also

argued that binary Ib/Ic progenitors are necessary to explain the observed SN fraction. A recent finding by Sana et al. (2012) shows that binary interaction may affect 70% or more of the massive star population.

Considering the two channels of high- and low-mass progenitors possible for SN Ib/Ic, it is interesting to compare it with the derived initial masses of the compact remnants in the Galaxy. Magnetars are believed to be formed by rapidly rotating massive stellar cores, and this mechanism would not work if the star enters the red supergiant phase where magnetic breaking between the stellar core and envelope may spin down the core rotation. Therefore, a very high mass star ($\gtrsim$40 $M_\odot$) that can lose a significant portion of its hydrogen envelope prior to SN is required as the progenitor of magnetars. Several studies have confirmed this by studying the host star clusters of the magnetars (e.g., Muno et al. 2006), but Davies et al. (2009) showed that the magnetar SGR 1900+14 may have had a low-mass progenitor of around 17 $M_\odot$. Therefore, the SN that produced those magnetars should also come from both massive and lower-mass stars, and the SN needs to be a stripped-envelope event to be able to produce rapid core rotation that eventually gave birth to the magnetar. In context with the SN Ib/Ic progenitor initial mass derived from our study, the two results are in line. More samples of both Ib/Ic SN and magnetar progenitors would be beneficial to establish a firm connection between the two.

We note that this study is based on the assumption that the SN progenitor was a member of the apparent host star cluster present at the explosion site. While this assumption might not necessarily be true, we argue that it is more likely that the associated cluster is the real parent stellar population of the SN progenitor rather than the diffuse background stellar population. The host cluster has been revealed to have a very young age, thus the IMF implies a higher probability of having high-mass stars compared to the background stellar population which is significantly older than the few megayear age of the prominent cluster. We discuss the probability of contamination by older, invisible clusters in the field in Paper II, where the effect is more important for SN II progenitors, which are presumably older than SN Ib/Ic progenitors.

We also present our mass estimate if we consider only the high-association cases, i.e., SNe within 150 pc of the host cluster center. This 150 pc is about the intermediate size between classical and giant H II regions (Crowther 2013), as most of our clusters are apparently around this size. With this limitation, the mean progenitor mass of SNe Ic reduces to $27.5 \pm 6.7\,M_\odot$, and SN Ib progenitors to $22.6 \pm 12.1\,M_\odot$. This would not change the aforementioned conclusion.

5. SUMMARY

We present the results of our investigation of nearby SNe Ib/Ic explosion sites using the IFS technique, performed using UH88/SNIFS and Gemini/GMOS. Taking advantage of IFS, we spatially identified star clusters at the explosion sites and extracted their respective spectra for the purpose of analysis. From the spectra we derived the metallicities of the clusters in terms of 12+log(O/H) using the strong-line method, and age using comparison of observed Hα emission EW with theoretical SSP models from Starburst99.

The method employed in this study offers the best available determination of SN progenitor natal metallicity, probing a very localized region, specifically, the parent stellar population from which the SN progenitor was born. This minimizes the effect of contamination from other populations and is definitely more reliable compared to metallicity determinations using proxies. As metallicity is one important parameter in the context of SNe Ib/Ic progenitor studies, our result provides an important insight in this field. We found evidence that the metallicity of SNe Ic explosion sites is on average higher than that of SNe Ib sites by $\sim$0.1 dex. This result is in accordance with Leloudas et al. (2011) and Sanders et al. (2012) who also found evidence that SN Ic explosion sites are more metal-rich compared to SN Ib sites, although not statistically significant, and Modjaz et al. (2011) who suggest the same conclusion with results they claim to be statistically significant.

The age of the SN progenitor host cluster is considered as the lifetime of the progenitor star. Compared with Padova stellar evolution models, we are able to derive the initial mass of SNe Ib/Ic progenitors from the ages of their parent star cluster. We found that SNe Ic explosion sites have a younger age than SNe Ib, indicating that they arise from higher-mass progenitors than SNe Ib. The derived progenitor mass from the host cluster age is significantly higher for SN Ic, over $42\,M_\odot$ versus $21\,M_\odot$ for SN Ib progenitors. We note that these derived average progenitor masses were derived from a sample that includes sub-WR mass progenitors ($\lesssim 25\,M_\odot$) which may be interpreted as binary progenitors. If we consider the single progenitors only, SN Ic progenitors average $47.9\,M_\odot$ while SN Ib progenitor mass average is $32.2\,M_\odot$—still attesting that SN Ic progenitors are the more massive ones. Further, if only SNe showing high association with the parent clusters are considered, the average progenitor mass estimates would reduce to 27.5 and 22.6, for SNe Ic and Ib, respectively.

In general, our findings support the current picture of stripped envelope (Ib/Ic) SN progenitors: SNe Ic tend to have more massive progenitors and are more metal-rich than SNe Ib, and for both SN types interacting massive binary stars may comprise a fraction of the progenitors of the SNe.

REFERENCES

Adamo, A., Smith, L. J., Gallagher, J. S., et al. 2012, MNRAS, 426, 1185
Aldering, G., Adam, G., Antilogus, P., et al. 2002, Proc. SPIE, 4836, 61
Aldering, G., Antilogus, P., Bailey, S., et al. 2006, ApJ, 650, 510
Aldering, G., Humphreys, R. M., & Richmond, M. 1994, AJ, 107, 662
Allington-Smith, J., Murray, G., Content, R., et al. 2002, PASP, 114, 892
Anders, P., & Fritze-v. Alvensleben, U. 2003, A&A, 401, 1063
Anderson, J. P., Covarrubias, R. A., James, P. A., Hamuy, M., & Habergham, S. M. 2010, MNRAS, 407, 2660
Anderson, J. P., Habergham, S. M., James, P. A., & Hamuy, M. 2012, MNRAS, 424, 1372
Anderson, J. P., & James, P. A. 2008, MNRAS, 390, 1527
Arribas, S., Mediavilla, E., García-Lorenzo, B., del Burgo, C., & Fuensalida, J. J. 1999, A&AS, 136, 189

Asplund, M., Grevesse, N., Sauval, A. J., Allende Prieto, C., & Kiselman, D. 2004, A&A, 417, 751
Bacon, R., Copin, Y., Monnet, G., et al. 2001, MNRAS, 326, 23
Barbon, R., Buondí, V., Cappellaro, E., & Turatto, M. 1999, A&AS, 139, 531
Baron, E., Young, T. R., & Branch, D. 1993, ApJ, 409, 417
Bastian, N., & Goodwin, S. P. 2006, MNRAS, 369, L9
Berg, D. A., Skillman, E. D., & Marble, A. R. 2011, ApJ, 738, 2
Bersten, M. C., Benvenuto, O. G., Nomoto, K., et al. 2012, ApJ, 757, 31
Blaylock, M., Branch, D., Casebeer, D., et al. 2000, PASP, 112, 1439
Boffi, F. R., Sparks, W. B., & Macchetto, F. D. 1999, A&AS, 138, 253
Boissier, S., & Prantzos, N. 2009, A&A, 503, 137
Bressan, A., Fagotto, F., Bertelli, G., & Chiosi, C. 1993, A&AS, 100, 647
Bressert, E., Bastian, N., Gutermuth, R., et al. 2010, MNRAS, 409, L54
Clocchiatti, A., Wheeler, J. C., Benetti, S., & Frueh, M. 1996, ApJ, 459, 547
Clocchiatti, A., Wheeler, J. C., Kirshner, R. P., et al. 2008, PASP, 120, 290
Crockett, R. M., Eldridge, J. J., Smartt, S. J., et al. 2008a, MNRAS, 391, L5
Crockett, R. M., Maund, J. R., Smartt, S. J., et al. 2008b, ApJL, 672, L99
Crockett, R. M., Smartt, S. J., Eldridge, J. J., et al. 2007, MNRAS, 381, 835
Crowther, P. A. 2007, ARA&A, 45, 177
Crowther, P. A. 2013, MNRAS, 428, 1927
Davies, B., Figer, D. F., Kudritzki, R.-P., et al. 2009, ApJ, 707, 844
Eldridge, J. J., Fraser, M., Smartt, S. J., Maund, J. R., & Crockett, R. M. 2013, MNRAS, submitted arXiv:1301.1975
Eldridge, J. J., Izzard, R. G., & Tout, C. A. 2008, MNRAS, 384, 1109
Eldridge, J. J., & Tout, C. A. 2004, MNRAS, 353, 87
Elias-Rosa, N., Van Dyk, S. D., Li, W., et al. 2011, ApJ, 742, 6
Fagotto, F., Bressan, A., Bertelli, G., & Chiosi, C. 1994, A&AS, 105, 29
Filippenko, A. V. 1982, PASP, 94, 715
Folatelli, G., & Morrell, N. 2009, CBET, 1807, 1
Fraser, M., Ergon, M., Eldridge, J. J., et al. 2011, MNRAS, 417, 1417
Gal-Yam, A., Fox, D. B., Kulkarni, S. R., et al. 2005, ApJL, 630, L29
Gaskell, C. M., Cappellaro, E., Dinerstein, H. L., et al. 1986, ApJL, 306, L77
Georgy, C., Meynet, G., Walder, R., Folini, D., & Maeder, A. 2009, A&A, 502, 611
Gerardy, C. L., Fesen, R. A., Nomoto, K., et al. 2002, PASJ, 54, 905
Gogarten, S. M., Dalcanton, J. J., Murphy, J. W., et al. 2009, ApJ, 703, 300
Heger, A., Fryer, C. L., Woosley, S. E., Langer, N., & Hartmann, D. H. 2003, ApJ, 591, 288
Hook, I. M., Jørgensen, I., Allington-Smith, J. R., et al. 2004, PASP, 116, 425
Howell, S. B., & Tonry, J. L. 2003, BAAS, 35, 1235
Hunter, D. J., Valenti, S., Kotak, R., et al. 2009, A&A, 508, 371
Immler, S., & Brown, P. J. 2008, ATel, 1481, 1
Immler, S., Brown, P. J., & Milne, P. 2008, ATel, 1463, 1
Kuncarayakti, H., Doi, M., Aldering, G., et al. 2013, AJ, 146, 31 (Paper II)
Kotulla, R., Fritze, U., Weilbacher, P., & Anders, P. 2009, MNRAS, 396, 462

Lada, C. J., & Lada, E. A. 2003, ARA&A, 41, 57
Lantz, B., Aldering, G., Antilogus, P., et al. 2004, Proc. SPIE, 5249, 146
Leitherer, C., Schaerer, D., Goldader, J. D., et al. 1999, ApJS, 123, 3
Leloudas, G., Gallazzi, A., Sollerman, J., et al. 2011, A&A, 530, A95
Maund, J. R., & Smartt, S. J. 2005, MNRAS, 360, 288
Maund, J. R., Smartt, S. J., Kudritzki, R. P., Podsiadlowski, P., & Gilmore, G. F. 2004, Natur, 427, 129
Maund, J. R., Smartt, S. J., & Schweizer, F. 2005, ApJL, 630, L33
Modjaz, M., Kewley, L., Bloom, J. S., et al. 2011, ApJL, 731, L4
Monard, L. A. G. 2009, CBET, 1798, 1
Muno, M. P., Clark, J. S., Crowther, P. A., et al. 2006, ApJL, 636, L41
Navasardyan, H., & Benetti, S. 2009, CBET, 1806, 1
Navasardyan, H., Benetti, S., Harutyunyan, A., et al. 2008, CBET, 1325, 1
Nomoto, K., Yamaoka, H., Pols, O. R., et al. 1994, Natur, 371, 227
Pérez-Montero, E., & Contini, T. 2009, MNRAS, 398, 949
Pettini, M., & Pagel, B. E. J. 2004, MNRAS, 348, L59
Podsiadlowski, P., Joss, P. C., & Hsu, J. J. L. 1992, ApJ, 391, 246
Portegies Zwart, S. F., McMillan, S. L. W., & Gieles, M. 2010, ARA&A, 48, 431
Porter, A. C. 1993, PASP, 105, 1250
Porter, A. C., & Filippenko, A. V. 1987, AJ, 93, 1372
Prantzos, N., & Boissier, S. 2003, A&A, 406, 259
Sahu, D. K., Gurugubelli, U. K., Anupama, G. C., & Nomoto, K. 2011, MNRAS, 413, 2583
Sana, H., de Mink, S. E., de Koter, A., et al. 2012, Sci, 337, 444
Sanders, N. E., Soderberg, A. M., Levesque, E. M., et al. 2012, ApJ, 758, 132
Sauer, D. N., Mazzali, P. A., Deng, J., et al. 2006, MNRAS, 369, 1939
Schlegel, E. M., & Kirshner, R. P. 1989, AJ, 98, 577
Smartt, S. J. 2009, ARA&A, 47, 63
Smartt, S. J., Eldridge, J. J., Crockett, R. M., & Maund, J. R. 2009, MNRAS, 395, 1409
Smith, N., Li, W., Filippenko, A. V., & Chornock, R. 2011, MNRAS, 412, 1522
Sramek, R. A., Panagia, N., & Weiler, K. W. 1984, ApJL, 285, L59
Stockdale, C. J., Weiler, K. W., Immler, S., et al. 2008, ATel, 1477, 1
Swartz, D. A., & Wheeler, J. C. 1991, ApJL, 379, L13
Tanaka, M., Kawabata, K. S., Maeda, K., Hattori, T., & Nomoto, K. 2008, ApJ, 689, 1191
Valenti, S., Fraser, M., Benetti, S., et al. 2011, MNRAS, 416, 3138
van Dyk, S. D. 1992, AJ, 103, 1788
Van Dyk, S. D., Davidge, T. J., Elias-Rosa, N., et al. 2012, AJ, 143, 19
Van Dyk, S. D., Li, W., & Filippenko, A. V. 2003, PASP, 115, 1
Vink, J. S., de Koter, A., & Lamers, H. J. G. L. M. 2001, A&A, 369, 574
Weiler, K. W., Sramek, R. A., Panagia, N., van der Hulst, J. M., & Salvati, M. 1986, ApJ, 301, 790
Whitmore, B. C., Chandar, R., Schweizer, F., et al. 2010, AJ, 140, 75